Eur Biophys J (1998) 27: 377–389

ARTICLE

Péter Nagy · György Vámosi · Andrea Bodnár
Stephen J. Lockett · János Szöllősi

Intensity-based energy transfer measurements in digital imaging microscopy

Received: 2 September 1997 / Revised version: 22 December 1997 / Accepted: 30 January 1998

Abstract Investigation of protein-protein associations is important in understanding structure and function relationships in living cells. Using Förster-type resonance energy transfer between donor and acceptor labeled monoclonal antibodies we can assess the cell surface topology of membrane proteins against which the antibodies were raised. In our current work we elaborated a quantitative image microscopic technique based on the measurement of fluorescence intensities to calculate the energy transfer efficiency on a pixel-by-pixel basis. We made use of the broad excitation and emission spectrum of cellular autofluorescence for background correction of images. In addition to the reference autofluorescence images (UV background) we recorded three fluorescent images (donor, acceptor and energy transfer signal) of donor-acceptor double labeled samples, and corrected for spectral spillage of the directly excited donor and acceptor fluorescence into the energy transfer image. After careful image registration we were able to calculate the energy transfer efficiency on a pixel-by-pixel basis. In this paper, we also present a critical comparison between results obtained with this method and other approaches (photobleaching and flow cytometric energy transfer measurements).

Based on a presentation at the EBSA European Biophysics Congress, Orléans, France, July 1997.

P. Nagy (✉) · G. Vámosi · A. Bodnár · J. Szöllősi
Department of Biophysics and Cell Biology,
University Medical School of Debrecen,
H-4012 Debrecen, Hungary
e-mail: nagyp@jaguar.dote.hu

A. Bodnár
Biophysical Research Group
of the Hungarian Academy of Sciences,
University Medical School of Debrecen,
H-4012 Debrecen, Hungary

S. J. Lockett
Lawrence Berkeley Laboratory, Berkeley, California

Key words Energy transfer · Protein association · Digital imaging microscopy · Background correction

Introduction

It was not until the 1980s that scientists began to acknowledge the importance of protein-protein interactions in the plasma membrane (Heldin 1995). Although generally applied biochemical and immunological approaches (cocapping, coprecipitation, chemical crosslinking) have given valuable insight into the topography of such interactions, they have several disadvantages. These include the application of extraction or isolation protocols that preclude the investigation of proteins in their natural environment and may disrupt their interaction or may artificially generate protein aggregation, especially in the case of abundant cell surface glycoproteins (Shivnan et al. 1992). In contrast, Förster-type resonance energy transfer (FRET) offers a suitable and convenient alternative, since it can be performed on live cells without major interference with the physiological condition of the cells. FRET is a process by which an excited donor dye passes its energy to a nearby acceptor dye without radiation. The energy transfer efficiency, which is a function of the inverse sixth power of the separation between the donor and the acceptor, changes steeply in the 2–10 nm range in the case of the fluorescent dyes employed in the present work (fluorescein and rhodamine). Therefore it can be used to assess molecular associations in this distance range (Eisinger 1976).

By labeling the cell with a donor- (e.g. fluorescein-) and an acceptor- (e.g. rhodamine-) tagged monoclonal antibody we can assess the association of the proteins against which the antibodies were produced (Szöllősi et al. 1989). Measurements in a fluorometer, where cell suspensions are used, cannot reveal cell-by-cell differences, and a contribution from dead cells, cellular debris and unbound, free fluorescent molecules can be present in the signal (Szöllősi et al. 1984). Flow cytometric approaches are superior to measurements in cell suspensions, since they

are able to dissect subpopulations in biological samples, unwanted cells and debris can be gated out, and because of the small illumination volume, the concentration of free dye molecules (if present) is negligible. By measuring three intensities from each individual cell flow cytometrically (quenched donor, acceptor excited directly and energy transfer using acceptor emission excited at a donor absorption wavelength) one can calculate the energy transfer on a cell-by-cell basis (Szöllősi et al. 1984; Trón et al. 1984). If we measure only the quenching of the donor fluorescence in the presence of the acceptor, we can only calculate the energy transfer on a population basis, since the donor fluorescence in the absence of the acceptor is not available for the same cell measured flow cytometrically.

Digital fluorescence microscopy, although statistically not as reliable as flow cytometry, can give pixel-by-pixel resolution, so one is able to detect differences e. g. in the association pattern of a protein in distinct parts of a single cell. One such approach is based on the different photobleaching kinetics of a fluorescent donor in the presence and absence of an acceptor (Jovin and Arndt-Jovin 1989). This approach is, however, very sensitive to environmental factors such as the local concentration of fluorochromes and oxygen (Song et al. 1995, 1996). Fluorescence intensity is much less sensitive to such factors. Intensity-based energy transfer measurements can be carried out in a fluorescence microscope by measuring the fluorescence intensity of the acceptor when the donor is excited. However, this is complicated by the fact that this fluorescence intensity has contributions from both the direct donor and acceptor fluorescence. By using special, narrow band pass filters, it is possible to minimize these overspilled intensities (Uster and Pagano 1986; Zhou et al. 1991), but intensity in the energy transfer channel will still depend on the concentration of the donor. This obstacle has partially been overcome by dividing the energy transfer intensity by the direct donor fluorescence in the presence of acceptor (Liang et al. 1993), but this method gives only semi-quantitative results.

Correction for background (or autofluorescence) is yet another problem. Several methods have been applied previously that used reducing or quenching agents to decrease autofluorescence (Beisker et al. 1987; Hallden et al. 1991), or used red-shifted fluorescent dyes to decrease the relative autofluorescence intensity (Loken et al. 1987), or dyes with long lifetimes to be able to discriminate the useful signal from the short-lived background fluorescence (Seveus et al. 1994). These methods require either special instrumentation or special chemicals. Cell-by-cell background compensation has been used in flow cytometry (Alberti et al. 1987; Steinkamp and Stewart 1986). Another approach utilizes the broad excitation and emission spectra of cellular autofluorescence. We have previously applied this method to image cytometry to get rid of the high autofluorescence in specimens labeled for fluorescence in situ hybridization (Szöllősi et al. 1995).

In this study we devised a method that is able to give accurate energy transfer values on a pixel-by-pixel basis. We successfully applied our above-mentioned background correction method for energy transfer microscopy. Taking account of spillage between different fluorescent images, we calculated the energy transfer efficiency between the heavy chain of MHC-I and the β_2-microglobulin, and the MHC-I and MHC-II proteins. We compare our intensity-based results with those obtained by photobleaching energy transfer measurements and flow cytometric energy transfer measurements.

Materials and methods

Cells and antibodies

JY, a human B lymphoblastoid cell line, was obtained from the American Type Culture Collection (Rockville, MD) and grown according to its specification. W6/32 (anti human MHC-I antibody that binds to the heavy chain of the protein), L368 (anti human β_2-microglobulin) and L243 (anti human MHC-II) antibodies were prepared from supernatants of hybridomas. Antibodies against erbB2 (4D5 and 7C2) were a generous gift from Genentech Inc. (South San Francisco, CA).

Labeling of cells with antibodies

Aliquots of purified monoclonal antibodies were labeled with fluorescein-isothiocyanate (FITC) or tetramethylrhodamine-isothiocynate (TRITC, Molecular Probes, Eugene, OR) as described earlier (Szöllősi et al. 1989). Use of capital F and R refers to fluoresceinated and rhodaminated antibodies, respectively. Dye : protein ratios were determined separately for each antibody by spectrophotometric methods and were always between two and four. Labeled antibodies retained their binding capacity according to competition analysis using identical, unlabeled antibodies.

After harvest, cells were washed twice and resuspended in PBS. About 10^6 cells in 50 μL PBS were incubated with fluorescently tagged antibodies at saturating concentration (1–2 μM depending on the type of antibody) for 30 min on ice in the dark. The excess monoclonal antibody was removed by washing the cells in PBS twice. Cells were either used immediately for measurements or were fixed in 1% formaldehyde. Results obtained with live and fixed cells were identical within the accuracy of the measurements. Antibodies were centrifuged (at 100,000 g for 30 min) before use to avoid possible aggregation.

Flow cytometric energy transfer measurements

We used a modified Becton Dickinson FACStar Plus flow cytometer equipped with dual argon ion laser excitation to measure the energy transfer efficiency. A detailed description of the method has been given elsewhere (Szöllősi et al. 1984; Trón et al. 1984). Briefly, three fluorescence inten-

sities were measured. Two were excited at 488 nm and detected at 540 ± 20 nm and above 580 nm, respectively, and the third was excited at 514 nm and detected above 580 nm. Forward angle light scattering (at 514 nm) was used to gate out debris and dead cells. All data were stored in list mode format. We calculated the energy transfer efficiency (E) on a cell-by-cell basis from the three fluorescence intensities. "E" values are presented as mean values from approximately normally distributed, unimodal energy transfer histograms of 10,000 cells calculated from at least four independent measurements. The high number of measured cells in flow cytometric energy transfer (FCET) minimizes the distorting effects of biological variation in cell samples and antibodies on the calculated E values.

Photobleaching energy transfer measurements (pbFRET)

We used an Axioplan Zeiss microscope equipped with a MicroImager camera (Xillix Technologies Corp., Vancouver, British Columbia, Canada) and Scilimage software (The University of Amsterdam, The Netherlands) installed on a SUN workstation. The optical filters and dichroic mirrors used for fluorescein were those presented in Table 1. Energy transfer was calculated using the photobleaching energy transfer method, pbFRET (Jovin and Arndt-Jovin 1989; Szabó et al. 1995; Damjanovich et al. 1997). Briefly, photobleaching is an irreversible photochemical reaction that destroys the chemical structure of the dye. Because this reaction can only take place in the excited state, the rate at which the sample is bleached, is proportional to the time spent in the excited state. As energy transfer shortens this time, it slows down the rate of photobleaching. Photobleaching kinetics in regions of interest (ROIs) were measured on donor labeled and donor-acceptor double labeled samples. At the end of each experiment the sample was continuously illuminated for two minutes to determine the background. The residual intensity changed by less than 0.5% upon further illumination. This background was subtracted from all images on a pixel-by-pixel basis and the resulting bleaching curves were fitted to double exponential functions, which yielded the best result. From the two exponential time constants we calculated an effective photobleaching time constant by taking an amplitude weighted average (Young et al. 1994). Frequency histograms of the time constants for both the donor and donor-acceptor labeled samples were made and the means of the histograms were calculated. From these mean values the average energy transfer efficiency can be calculated (Jovin and Arndt-Jovin 1989):

$$E = 1 - \frac{T_D}{T_{DA}} \quad (1)$$

where T_D and T_{DA} are the mean effective bleaching time constants of the donor-only labeled and the donor-acceptor double-labeled sample, respectively. Averages calculated from the mean values of histograms from at least six independent measurement are presented in Table 3.

Table 1 Excitation filters, emission filters and dichroic mirrors for the measurement of fluorescein, rhodamine and energy transfer intensities

	Excitation	Dichroic	Emission
Background (I_{Bg})	365 nm BP	FT395	450±50 nm
Fluorescein (I_1)	490±10 nm	FT510	535±30 nm
Energy transfer (I_2)	490±10 nm	FT565	590 LP
Rhodamine (I_3)	546±12 nm	FT565	590 LP

Intensity-based energy transfer measurements

We used the same microscope and software as those used for pbFRET measurements. The excitation and emission filters and dichroic mirrors used to measure fluorescein, rhodamine and energy tranfer intensities are presented in Table 1.

Registration of images

Images recorded with different dichroic mirrors are usually shifted relative to each other. In addition, gradual shifts also occur during the course of longer measurements. In these cases image registration is necessary. We superimposed the images to be registered on each other and shifted one of them either manually or using an automated routine to achieve the best overlap. We found that the manual method is more reliable than the automated one (based on mean square errors) in cases when less bright or fuzzy images were to be registered. Automated routines were found to be most accurate with, for example, fluorescent beads with very sharp edges. In the case of images where fluorescence intensity was very low, we used fluorescent beads with wide excitation and emission spectra for registration (Multispeck™ from Molecular Probes, Eugene, OR).

Absorption and fluorescence excitation spectra of the dyes conjugated to antibodies

The absorption spectra of fluorescein and rhodamine conjugated to antibodies were recorded on a Shimadzu UV-2100 spectrophotometer with 0.5 nm step size. The extinction values $\varepsilon(\lambda)$ were determined by assuming molar extinction values of $\varepsilon_F = 73{,}000\ M^{-1}\ cm^{-1}$ and $\varepsilon_R = 83{,}000\ M^{-1}\ cm^{-1}$ based on the peak absorption values provided by the manufacturer (Molecular Probes, Eugene, OR).

Corrected fluorescence excitation spectra were taken on a Perkin Elmer MPF-44B spectrofluorometer. The fluorescein and rhodamine spectra were normalized by setting the maxima equal to the extinction maxima of the corresponding dye.

Determination of the spectral characteristics of the optical elements

For the calculation of the total absorption of the dyes the spectral properties of the optical elements of the excitation pathway of the microscope were measured with a Shimadzu UV-2100 spectrophotometer. The transmission spectrum of the excitation filter and the dichroic mirrors (the latter placed at 45° with respect to the illumination beam) were measured with a step size of 0.5 nm. The reflectance, R, of the dichroic mirrors was calculated as $R = 1 - T$, where T is the transmission. The energy per unit wavelength vs. wavelength spectra, $I_E(\lambda)$, of the Hg arc lamps were acquired from the manufacturer (Osram, Germany). The relative photon number per unit wavelength vs. wavelength spectrum, $I_N(\lambda)$, was calculated as $I_N(\lambda) \propto I_E(\lambda) \cdot \lambda$, where λ is the wavelength.

Results

Background correction of images

Background arises from several, quite distinct phenomena. It is partly generated by the "dark current" of the camera. To correct for this, we recorded fluorescent images for a given duration. Then we repeated the image acquisition with closed shutters for the same time. This is the "dark current" image. Afterwards we subtracted the "dark current" image from the fluorescent image on a pixel-by-pixel basis. All the intensities in the equations presented refer to "dark current" corrected intensities.

The second component of the background is caused by the fluorescence of the optical elements of the microscope and the slide or coverslip (this component is important in the case of cells grown on coverslips, because the glass surface is covered by proteins). This is determined by measuring the average pixel values in cell free areas on each sample (boxes with dashed lines in Fig. 1). The values of at least 2–3 boxes are averaged in each image, and this constant value is subtracted from each pixel in the given image.

The third component of background is due to autofluorescence of the cells. Since the autofluorescence spectrum of cells has a wide excitation and emission spectrum and is fairly constant, it is possible to define ratios (B_1 to B_3) that describe the ratio of fluorescence intensities recorded with the fluorescein (B_1), energy transfer (B_2) and rhodamine (B_3) filter and dichroic mirror sets to the fluorescence intensity called "background intensity" in our terminology recorded with UV excitation (for wavelengths see Table 1).

$$B_x = \frac{I_x}{I_{\text{UV background}}}, \quad x = 1, 2, 3 \tag{2}$$

These ratios are determined with unlabeled cells (Table 2). The high value of B_3 is the result of the high sensitivity of our camera in the red region. Although emission is also measured within the red region in the case of I_2, the excitation and emission wavelengths are very far from each other, and fluorescent molecules (including those responsible for cellular autofluorescence) do not usually exhibit such a big Stokes shift. Calculation of B_x values is not carried out on a pixel-by-pixel basis, but rather we sum the pixel values in the images, since the fluorescence intensities in single pixels are sometimes very low. Some bright

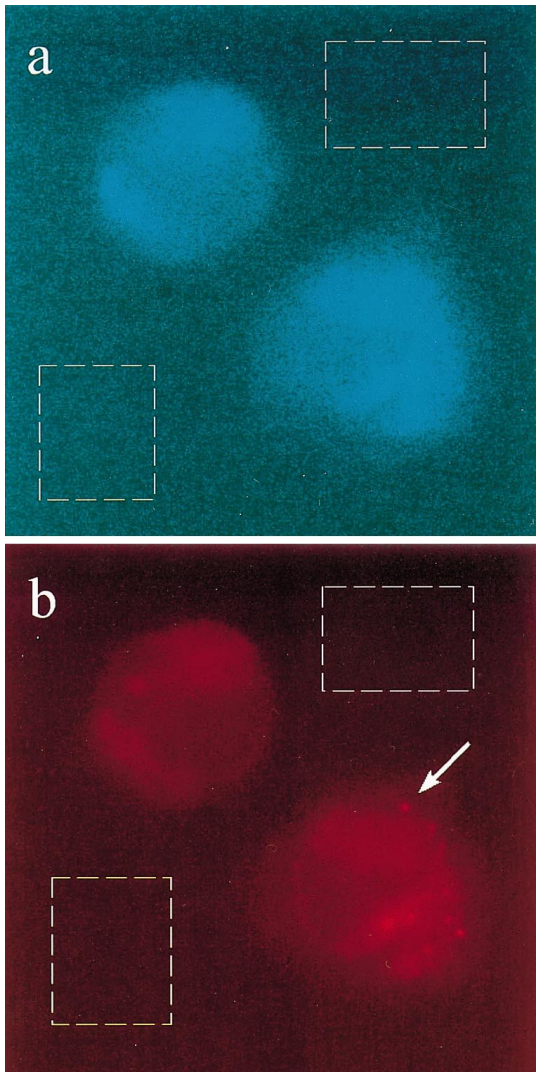

Fig. 1 a, b Background correction for energy transfer microscopy. **a** UV-excited background image of unlabeled cells. **b** Unlabeled cells recorded with the rhodamine filter and dichroic set. To correct for the autofluorescence of the slide and the optical elements of the microscope we select cell-free areas (*boxes* with *dashed lines* in **a** and **b**), and calculate the average pixel intensity of the boxes in each separate image. Then this constant value is subtracted from each pixel in the image. To calculate the spectroscopic $B_1 - B_3$ factors that characterize the spillage of the UV-excited background fluorescence intensity into the fluorescein, energy transfer and rhodamine images, respectively, we use unlabeled cells and select image areas where cells can be found. We sum the fluorescence intensity of the cells in the fluorescein, energy transfer and rhodamine images. Then we divide these values by the summed intensity of the same cells in the background channel to obtain the $B_1 - B_3$ factors. Bright spots (marked by an *arrow* in image **b**) are omitted from the calculations

Table 2 Spectroscopic and instrumental factors for the calculation of intensity-based energy transfer in microscopy

S_1	0.156±0.007	B_1	0.191±0.022
S_2	0.054±0.005	B_2	0.211±0.026
S_3	0*	B_3	1.857±0.362
S_4	0.011±0.003	α	0.59 ±0.08

The mean and SD values of the *S* and *B* factors, and of α are presented in this table. These values were used for the calculation of energy transfer in Fig. 4 and Table 3. * The value of S_3 was not calculated since the intensity in the rhodamine image (I_3) in the case of a fluorescein-labeled sample was not discernable from the background

spots (marked with an arrow in Fig. 1) in the background recorded with the rhodamine filters are neglected, since they are not present in the UV-excited image and would distort the calculation of the *B* factors. As the *B* factors do not contain the contribution from these very bright spots, similar shiny dots are also neglected in all of the images.

With the *B* factors known, we can background correct our fluorescence images. A UV-excited background image is recorded with the antibody labeled samples. After dark current and constant background (autofluorescence of the slide and the optical elements) correction on the background and the fluorescein, energy transfer and rhodamine images, the following compensation is carried out on a pixel-by-pixel basis:

$$I_x \text{ (without cellular autofluorescence)} = I_x \text{ (with cellular autofluorescence)} - B_x \cdot I_{Bg} \quad (3)$$

where I_x stands for I_1 to I_3 (fluorescein, energy transfer and rhodamine intensities, respectively), I_{Bg} is the UV-excited background and B_x is the ratio described above. This is valid because our fluorescent dyes have negligible absorption in the relevant UV range. This correction eliminates the contribution of the autofluorescence from the I_1 to I_3 intensities from the individual pixels. It is worth noting that cellular autofluorescence ($B_x \cdot I_{Bg}$) amounted to about 10–15% of the total signal.

Theory of intensity-based energy transfer microscopy

In microscopy, intensity-based energy transfer determination is usually based on the measurement of sensitized emission of the acceptor. This is achieved by exciting the donor (fluorescein) and measuring the fluorescence emission from the acceptor (rhodamine, I_2 in equations below). This is, however, complicated by the fact that I_2 has a background component ($B_2 \cdot I_{Bg}$), and a contribution from the direct emission of the donor ($I_F \cdot (1–E) \cdot S_1$) and the acceptor ($I_R \cdot S_2$). To overcome this problem, one has to measure four independent images of the same field. One intensity is the autofluorescence of cells that is excited in the UV range where the fluorescent labels used have negligible absorbtion (I_{Bg}). Since the background intensity that can be measured using this UV excitation is rather low, the acquisition time for this image was usually long (3–5 sec) and we used a wide emission filter. Exposure times for the fluorescein, energy transfer and rhodamine images were 1–2 seconds depending on the signal. These intensities are presented below:

$$I_1(490, 535) = B_1 \cdot I_{Bg} + I_F \cdot (1–E) + I_R \cdot S_4 \quad (4)$$

$$I_2(490, >590) = B_2 \cdot I_{Bg} + I_F \cdot (1–E) \cdot S_1 + + I_R \cdot S_2 + I_F \cdot E \cdot \alpha \quad (5)$$

$$I_3(546, >590) = B_3 \cdot I_{Bg} + I_F \cdot (1–E) \cdot S_3 + I_R \quad (6)$$

In the above equations I_F is the unquenched fluorescein intensity, I_R is the direct rhodamine emission. The numbers in brackets refer to the wavelengths of excitation and emission in the case of the given intensity (for filters and dichroic mirrors consult Table 1). The I_1, I_2 and I_3 intensities are usually referred to as fluorescein, energy transfer and rhodamine images or intensities, respectively, although these intensities contain contributions from other sources, as well. The S_1–S_4 factors characterize the spectral overlap between different channels (Table 2). S_1 and S_3 are determined using samples labeled only with fluorescein according to the following equations (Trón et al. 1984):

$$S_1 = \frac{I_2}{I_1}, \quad S_3 = \frac{I_3}{I_1} \quad (7, 8)$$

Fortunately using our filter and dichroic mirror setup S_3 was zero, making Eqs. (4)–(6) simpler. In spite of this we retained this designation to make our equations compatible with those of the flow cytometric approach (Trón et al. 1984). S_2 and S_4 are determined on samples labeled only with rhodamine according to the following equations:

$$S_2 = \frac{I_2}{I_3}, \quad S_4 = \frac{I_1}{I_3} \quad (9, 10)$$

We neglect the small amount of fluorescence intensity that may be present in I_1 due to the spillage of sensitized rhodamine emission into the I_1 channel ($I_F \cdot E \cdot \alpha \cdot S_4/S_2$), which is about 2% of I_F even when $E = 20\%$, and it amounts to even less of the total I_1 intensity.

The fluorescence intensities in Eqs. (7)–(10) represent summed fluorescence intensities from the same part of the images. For example, to calculate S_1 some bright cells are selected, and the intensity of these cells is summed in the energy transfer (I_2) and the fluorescein (I_1) image. The proportionality factor α is the ratio of the fluorescence intensity of a given number of excited rhodamine molecules measured in the I_2 channel to the fluorescence intensity of the same number of excited fluorescein molecules detected in the I_1 channel. This is constant for a given experimental setup and a particular pair of donor and acceptor conjugated ligands and must be measured for every defined case. The determination of α will be described below.

When we calculate the energy transfer values using the intensity-based approach, we have to correct for photobleaching. Since the bleaching rate of rhodamine is very low with our illumination intensities, we had to use this

correction only for the fluorescein and the energy transfer images. We sequentially recorded fluorescein and energy transfer images repeatedly. We used a linear approximation of bleaching which is reasonable for short exposure times: when calculating the energy transfer in an image, we computed the relevant fluorescein intensity as the average of the previous and the next fluorescein image.

Image processing

The calculation of energy transfer begins with image registration to correct for shifts between image recordings. Then we usually gate on high intensity parts of the images, since reliable calculation can only be done in these parts, because the energy transfer part of I_2 ($I_F \cdot E \cdot \alpha$) usually accounts for only a small percentage (10–20%) of the total I_2. Sometimes, if the intensity is low, compression of the images by pooling the signals of neighboring pixels is necessary to increase the pooled intensity to an appropriate level. Of course, this is done at the expense of spatial resolution. Then we subtract the constant background (autofluorescence of optical elements and the slide), determined in an area with no cells. Afterwards we subtract cellular autofluorescence from each image ($B_x \cdot I_{Bg}$, $x = 1, 2, 3$). In this way the corrected I_3 image will be equal to I_R. Then subtraction of $S_4 \cdot I_R$ from the fluorescein image is carried out leaving $I_F \cdot (1-E)$. Subtraction of the fluorescein contribution ($I_F \cdot (1-E) \cdot S_1$) from the energy transfer image (I_2) leaves $I_R \cdot S_2 + I_F \cdot E \cdot \alpha$, which is the direct plus sensitized emission of the acceptor (F_{AD}). We can proceed in two ways from here:

1., $I_R \cdot S_2$ is subtracted from the energy transfer image, and the remaining $I_F \cdot E \cdot \alpha$ is divided by $(I_1 - B_1 \cdot I_{Bg} - I_R \cdot S_4) \cdot \alpha = I_F \cdot (1-E) \cdot \alpha$. This gives $E/(1-E)$ which is β in Eq. (11):

$$\frac{I_2 - B_2 \cdot I_{Bg} - (I_1 - B_1 \cdot I_{Bg}) \cdot S_1 + (I_3 - B_3 \cdot I_{Bg}) \cdot (S_1 \cdot S_4 - S_2)}{\alpha \cdot (I_1 - B_1 \cdot I_{Bg} - (I_3 - B_3 \cdot I_{Bg}) \cdot S_4)} = \beta \tag{11}$$

In the denominator we have the I_1 image corrected for background and rhodamine contribution multiplied by α. In the numerator we have the I_2 image corrected for background and fluorescein contribution ($I_2 - B_2 \cdot I_{Bg} - (I_1 - B_1 \cdot I_{Bg}) \cdot S_1$ and the background corrected I_3 image multiplied by $S_1 \cdot S_4 - S_2$.

2., E can be calculated according to the classical equation:

$$\frac{F_{AD}}{F_A} = 1 + \frac{A_D \cdot c_D}{A_A \cdot c_A} \cdot E \tag{12}$$

where F_A is the direct acceptor fluorescence (in our case $I_R \cdot S_2$) measured at the same excitation wavelength as the sensitized emission, A_D and A_A are the integrated absorptions of the donor and the acceptor in the fluorescein excitation range, respectively, c_D and c_A are the concentrations of the donor and the acceptor, respectively. Solving this equation gives

$$\left(\frac{I_2 - B_2 \cdot I_{Bg} - (I_1 - B_1 \cdot I_{Bg} - (I_3 - B_3 \cdot I_{Bg}) \cdot S_4) \cdot S_1}{(I_3 - B_3 \cdot I_{Bg}) \cdot S_2} - 1 \right) \cdot \frac{A_A \cdot c_A}{A_D \cdot c_D} = E \tag{13}$$

To be able to calculate E according to Eq. (13), we need to calculate the absorption ratio (A_A/A_D) and the pixel-by-pixel acceptor-donor ratio (c_A/c_D). Calculation of these values will be discussed below in separate sections.

Determination of α

α is a constant in our calculations that determines the proportion of the rhodamine to the fluorescein signal when the number of excited molecules is the same for both the fluorescein and rhodamine images. Owing to energy transfer $N \propto I_F \cdot E$ excited molecules are lost on the donor side, and an equal number of excited molecules appear on the acceptor side. α characterizes the ratio of the fluorescence quantum efficiencies of the donor and acceptor and the efficiency of the detection system at the two wavelengths.

For the determination of α, one needs a sample that is labeled with the same number of donor and acceptor antibodies. This can be achieved with an antibody pair, that binds to two, non-competing epitopes on the same protein and there should be no energy transfer between them. One such candidate is the 4D5 and 7C2 pair, that recognizes two, non-overlapping epitopes on the erbB2 protein (erbB2 is a member of the epidermal growth factor receptor family transmembrane tyrosine kinases, and it is often overexpressed in breast cancer). Other antibody pairs can also be used. When one such antibody pair is found, it can be used in any measurement with the same dyes, since α is determined by instrumental parameters and the spectral properties of the dyes.

We measure the fluorescein (I_1), energy transfer (I_2) and rhodamine (I_3) intensity of the cells labeled with both fluoresceinated 4D5 and rhodaminated 7C2 antibodies along with the UV-excited background image (I_{Bg}). After background correction of all images, we subtract $(I_3 - B_3 \cdot I_{Bg}) \cdot S_4$ from the I_1 image (that is the rhodamine spillover to the I_1 channel). Afterwards we subtract the resulting I_1 image from the I_2 image. In this way, the corrected I_1 image contains I_F (since $E = 0$), and the corrected I_2 image is $I_R \cdot S_2$. Then we sum the intensities of the images and divide the rhodamine intensity by the fluorescein intensity. In addition, we have to correct for the different labeling ratios of the antibodies and the different absorption of the two dyes:

$$\begin{aligned} \alpha &= \frac{\Phi_{0A} \cdot \eta_{em,A}}{\Phi_{0D} \cdot \eta_{em,D}} \\ &= \frac{I_2(\text{corrected})}{I_1(\text{corrected})} \cdot \frac{\int \varepsilon_D \cdot I_N \cdot T_{ex,F} \cdot R_{dic,F} \cdot \mathrm{d}\lambda}{\int \varepsilon_A \cdot I_N \cdot T_{ex,F} \cdot R_{dic,R} \cdot \mathrm{d}\lambda} \cdot \frac{L_D}{L_A} \\ &= \frac{I_2(\text{corrected})}{I_1(\text{corrected})} \cdot \frac{A_D}{A_A} \cdot \frac{L_D}{L_A} \end{aligned} \tag{14}$$

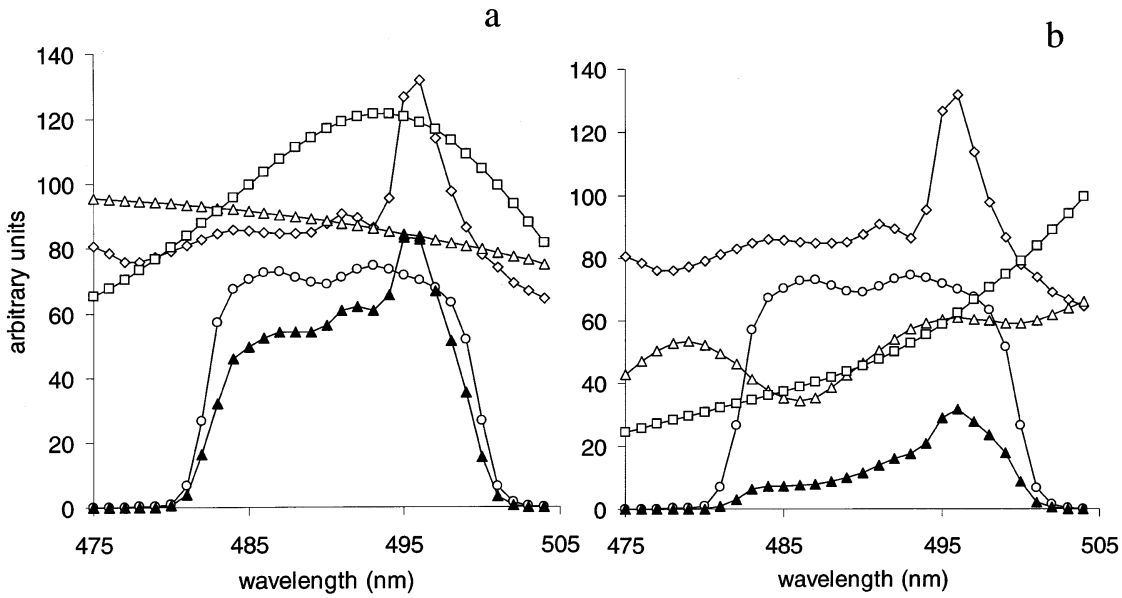

Fig. 2 Determination of the absorption ratio. Emission spectrum of the Hg arc lamp (◇), transmission profiles of the fluorescein excitation filter (○), reflection spectra of the fluorescein and the rhodamine dichroic mirrors (△), and absorption spectra of the fluoresceinated and rhodaminated antibodies (□) were measured for the fluoresceinated (part *a*) and rhodaminated (part *b*) antibodies. Then we multiplied these factors together to obtain the curve marked by ▲. The area under these curves is proportional to the absorption of these dyes using the given filter sets

Φ_{0A} and Φ_{0D} are the fluorescence quantum yields of the donor and the acceptor in the absence of external quenching mechanisms, $\eta_{em,A}$ and $\eta_{em,D}$ are the transmission and detection efficiencies of the emission pathway in the donor and acceptor channels. ε_D and ε_A are the molar absorption coefficients of fluorescein and rhodamine, respectively, I_N is the number of photons in the exciting beam, $T_{ex,F}$ is the transmission of the fluorescein excitation filter, $R_{dic,F}$ and $R_{dic,R}$ are the reflectances of the fluorescein and rhodamine dichroic mirrors, respectively. $T_{ex,F}$ appears in the denominator as well as in the numerator, since the I_2 intensity is excited in the fluorescein excitation range. L_D and L_A are the labeling ratios of the antibodies (the number of fluorescent molecules on a single immunoglobulin). A_D and A_A are proportional to the number of photons absorbed per unit time by the donor and the acceptor, respectively. We can also calculate I_2 (corrected) by multiplying the background corrected rhodamine image by S_2.

If we are not lucky enough to find an antibody pair that binds to the same protein (to ensure an equal number of donor and acceptor antibodies) and gives no energy transfer, we can use other, non-competing antibodies against the same protein. In this case, however, we have to take the energy transfer into account. Since energy transfer values between different epitopes of the same protein are pretty constant, we can use the energy transfer value from flow cytometric measurements to calculate the unquenched fluorescein intensity:

$$I_F = \frac{I_1 - B_1 \cdot I_{Bg}}{1 - E} \tag{15}$$

We write I_F in place of I_1 (corrected) and $(I_3 - B_3 \cdot I_{Bg}) \cdot S_2$ in place of I_2 (corrected) in Eq. (14).

Determination of the absorption ratio (A_D/A_A)

Because the light source (mercury arc lamp) has a continuous spectrum, the amount of light absorbed by a dye is determined by the spectral characteristics of the optical elements and the absorption spectrum of the dye over a finite wavelength range. The spectrum of the mercury arc lamp was obtained from the manufacturer, while the transmission of the excitation filter (fluorescein filters were used for both antibodies), the reflection of the two dichroic mirrors and the absorption spectra of a fluoresceinated (F-W6/32) and a rhodaminated (R-KE2) antibody were recorded on a spectrophotometer. Then the product of these was calculated separately for the fluoresceinated and the rhodaminated antibodies over the spectral range where the product differs from zero (Fig. 2). These quantities have been rescaled to fit into the same coordinate system while maintaining their relative values between the pairs for fluorescein and rhodamine. The area under the curve of the product is proportional to the total amount of photons absorbed by the dye. The ratio of these areas for the two dyes is the relevant absorption ratio.

We can measure the absorption of the acceptor in the same wavelength range as that used for fluorescein excitation in a similar way using the rhodamine filter for excitation and calculating the product described above. Multiplication of this product by S_2 gives the absorption of rhodamine in the fluorescein excitation range.

The absorption ratio was also determined using fluorescence excitation spectra of the dyes rather than the absorption spectra. These spectra have somewhat different shapes in the case of rhodamine. The appearance of a peak in the absorption spectrum of the antibody-conjugated dye that has no corresponding peak in the excitation spectrum indicates the formation of dark complexes between the dye and the antibody. In this way the final value of the absorption ratio was different for the two cases, so the energy transfer values determined using these absorption ratios also differed accordingly. This is similar to the situation where energy transfer values are not the same when determined from the quenching of the donor or the sensitized emission of the acceptor.

Determination of the donor-acceptor ratio on a pixel-by-pixel basis

For the determination of the local donor-acceptor concentration on donor-acceptor double labeled samples we first calculate the direct fluorescein (I_F) and rhodamine intensities (I_R). Then we have to convert this fluorescence intensity ratio to a concentration ratio. Therefore we need a calibration constant that characterizes the fluorescence intensity ratio I_R/I_F in the case of an equal number of fluorescein and rhodamine molecules.

For the determination of this constant one also requires cells with the same number of fluoresceinated and rhodaminated antibodies bound without energy transfer. We record a fluorescein (I_1) and a rhodamine (I_3) image. Then these images are corrected for background and the fluorescein image is corrected for direct rhodamine contribution to give I_1 (corrected) and I_3 (corrected). Afterwards we take the ratio of the summed corrected rhodamine intensity (I_3) and the corrected fluorescein intensity (I_1) of the same cells. Then we have to correct for the different labeling ratios of the antibodies to obtain a constant: the ratio of the rhodamine and fluorescein signals when the number of fluorescein and rhodamine molecules are the same:

$$C = \frac{\sum_j I_{3j}(\text{corrected})}{\sum_j I_{1j}(\text{corrected})} \cdot \frac{L_F}{L_R} \tag{16}$$

where C is the calibration constant, while L_F and L_R are the labeling ratios of the antibodies determined from their absorption spectra. If we do not have a non-competing antibody pair against the same protein that gives no energy transfer, then we correct the fluorescein intensity for the energy transfer (Eq. (15)).

Afterwards in the case of energy transfer samples, we divide the fluorescein image (I_1)corrected for background and direct rhodamine fluorescence, I_1(corrected), by the background-corrected rhodamine image, I_3(corrected), and multiply the resulting image by the above constant. In this way, we obtain an image which contains the real donor/acceptor ratio on a pixel-by-pixel basis:

$$\frac{c_{Di}}{c_{Ai}} = \frac{I_{1i}(\text{corrected})}{I_{3i}(\text{corrected})} \cdot C \tag{17}$$

where c_{Di}/c_{Ai} is the donor/acceptor ratio. In our calculations we neglect the fact that, in the case of the energy transfer sample, the corrected I_1 intensity is the quenched fluorescence of the donor, and not I_F. This can be taken into account by solving the following set of equations:

$$I_1 = B_1 \cdot I_{Bg} + I_F \cdot (1-E) + I_R \cdot S_4 \tag{18}$$

$$I_2 = B_2 \cdot I_{Bg} + I_F \cdot (1-E) \cdot S_1 + F_{AD} \tag{19}$$

$$I_3 = B_3 \cdot I_{Bg} + I_R \tag{20}$$

$$\frac{F_{AD}}{F_A} = 1 + \frac{A_D \cdot c_D}{A_A \cdot c_A} \cdot E \tag{21}$$

$$\frac{c_D}{c_A} = \frac{I_F}{I_R} \cdot C \tag{22}$$

From the above equations we get

$$\beta = \left(\frac{I_2 - B_2 \cdot I_{Bg} - I_{1C}}{(I_3 - B_3 \cdot I_{Bg}) \cdot S_2} - 1 \right) \cdot \frac{A_A}{A_D} \cdot \frac{I_3 - B_3 \cdot I_{Bg}}{C \cdot I_{1C}} \tag{23}$$

where $\beta = E/(1-E)$ and $I_{1C} = I_1 - B_1 \cdot I_{Bg} - I_R \cdot S_4 = I_F(1-E)$.

Comparison of results obtained by different energy transfer calculation methods

We labeled cells with fluoresceinated anti β_2-microglobulin (F-L368) and rhodaminated anti MHC-I heavy chain antibodies (R-W6/32), or F-W6/32 and rhodaminated anti-MHC-II antibodies (R-L243), and analyzed cells from the same labeling with flow cytometric, photobleaching energy transfer, and the two intensity-based image microscopic methods described here (Table 3, Figs. 3 and 4). MHC-I and MHC-II proteins are important molecules in

Table 3 Comparison of different energy transfer calculation methods

Antibodies	Flow cytometer	pbFRET	Intensity-based, using α	Intensity-based, using F_{AD}
FL368+RW6/32	15±1%	22±3%	15±3%	17±2%
FW6/32+RL243	9±2%	14±3%	4±1%	4±2%
FW6/32+RL243 (low c_A)	ND	8±2%	3±1%	3±1%
FW6/32+RL243 (medium c_A)	ND	18±2%	10±1%	10±2%
FW6/32+RL243 (high c_A)	ND	24±3%	14±3%	15±2%

Samples from the same labeling were measured using the flow cytometric, photobleaching and intensity-based microscopic energy transfer calculation methods. ND = not determined

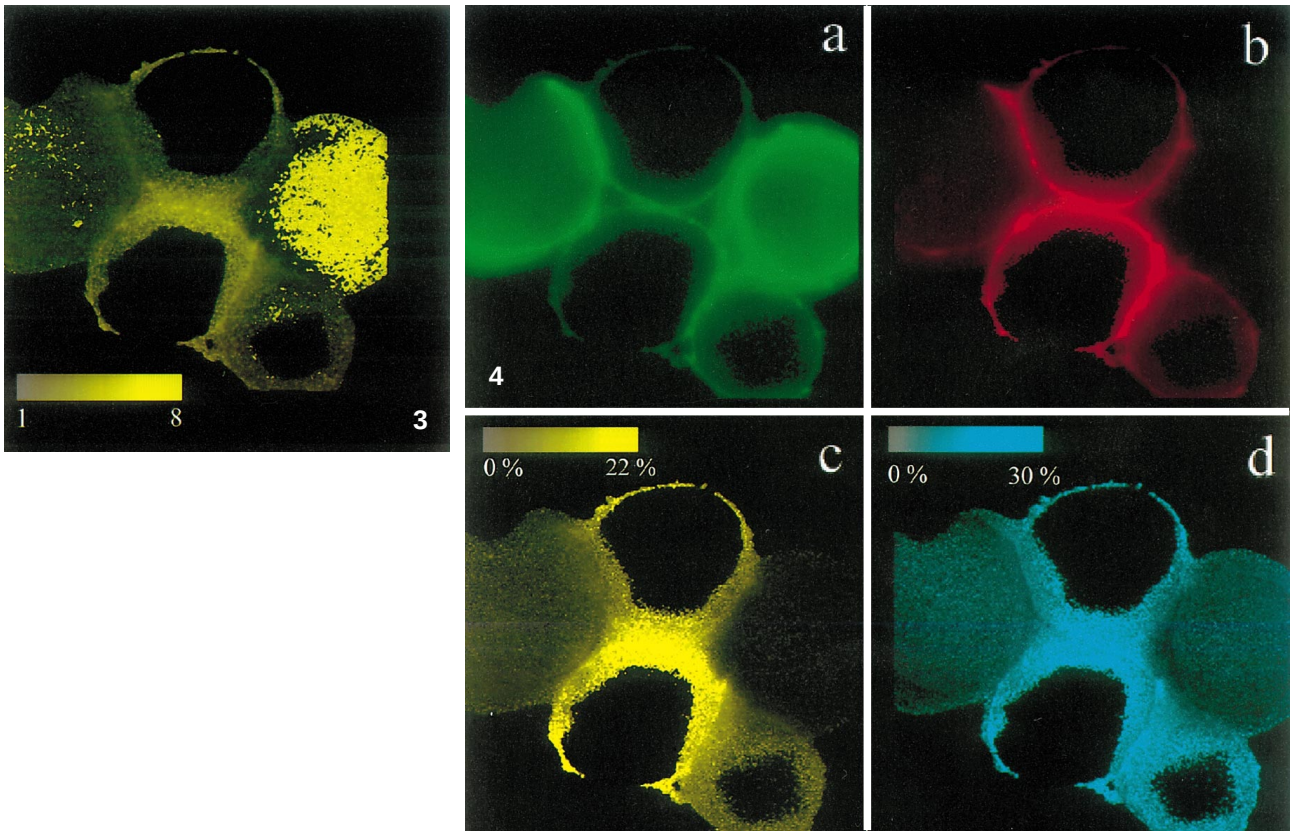

Fig. 3 Direct plus sensitized emission of the acceptor divided by the direct emission. JY cells were labeled with F-W6/32 and R-L243 antibodies, and the F_{AD}/F_A ratio was calculated (without any correction for donor-acceptor ratio). Bright pixels correspond to high values of the ratio. The displayed range of the ratio is between 1 and 8

Fig. 4 a–d Calculation of energy transfer on a pixel-by-pixel basis on JY cells labeled with F-W6/32 and R-L243. **a** Fluorescein image of JY cells labeled with F-W6/32 antibodies against the MHC-I protein. **b** Rhodamine image of JY cells labeled with R-L243 antibodies against MHC-II. **c** Intensity-based energy transfer image. Pixel values represent the energy transfer between F-W6/32 and R-L243 antibodies. **d** Photobleaching energy transfer image of the same cells. In the energy transfer images bright pixels correspond to high energy transfer

the interaction of cells of the immune system with each other and with their target cells.

The ratio F_{AD}/F_A (direct plus sensitized emission of the acceptor divided by the direct emission of the acceptor without any correction for donor-acceptor ratio) is not a good approximation of the energy transfer in the case of cells with huge differences in donor concentration (Fig. 3). Part *a* and part *b* of Fig. 4 are the fluorescein and rhodamine images of cells labeled with F-W6/32 and R-L243 antibodies, respectively. Since these antigens are expressed independently, there is a significant cell-by-cell variation in the relative amount of these proteins. Part *c* of Fig. 4, is an intensity-based energy transfer image calculated according to Eq. (13). Part *d* of the same figure is the pbFRET image. There is fairly good correlation between the two energy transfer images. However, it is worthwhile to compare Fig. 3 with Fig. 4*c*. In Fig. 3, where F_{AD}/F_A is presented, we can see that the highest pixel values can be found in pixels where the donor concentration is the highest. On the other hand, in part *c* of Fig. 4, energy transfer values are biggest in pixels with the highest acceptor concentration.

Results obtained by the different methods were consistent with theory: by selecting cells with different acceptor concentrations in the same microscopic field the calculated energy transfers were higher in the case of cells with high acceptor concentration (Table 3). The two intensity-based microscopic energy transfer methods yield the same energy transfer values within experimental error. In the case of the F-W6/32-RL243 antibody pair, there is a pronounced difference between the flow cytometric and image microscopic energy transfer values. These two cell surface proteins are expressed independently, so there is a big cell-by-cell variation in the relative amount of these proteins. This may increase the error in the mean energy transfer values in microscopic measurements where the number of measured cells is small. On the other hand, microscopic intensity-based energy transfer calculations are reliable with high fluorescence intensities. That is why we usually select bright cells, and this procedure may inadvertently introduce a bias towards cells that have a high number of fluoresceinated antibodies bound, and consequently possibly a low acceptor concentration. The correspondence between the microscopic approaches and the flow cytometric

method is very good in the case of the FL368-RW6/32 pair. These antibodies bind to different subunits of the same protein (MHC-I molecule). Since the conformation of MHC-I is not believed to display any cell-by-cell heterogeneity, the small number of cells sampled by energy transfer microscopy would not introduce a big uncertainty into the measurements. However, pbFRET gives a higher energy transfer value even in this case. We often experienced similar phenomena with other antibody pairs. We started to look for possible factors that make the two measurements inherently different. One such, previously unacknowledged factor, is the different weighting of pixel-by-pixel energy transfer values in intensity-based and photobleaching energy transfer measurements.

Differences in weighting of energy transfer values in pbFRET and in intensity-based energy transfer microscopy

In the case of intensity-based energy transfer measurements, energy transfer is measured on a pixel-by-pixel basis. To calculate the average energy transfer for a single cell, these values are averaged:

$$\bar{E}_{\text{INTENSITY}} = \frac{\sum_i E_i}{n} = \sum_{k_t} \frac{k_t}{k_n + k_f + k_t} \cdot n(k_t) \tag{24}$$

where k_n, k_f and k_t are the rate constants for non-fluorescent, fluorescent and energy transfer relaxations. Summation is over all existing values of k_t. The fraction of pixels with a given k_t is designated by $n(k_t)$. Variation in k_n and k_f is supposed to be negligible as compared to that in k_t. Here we do not weight the energy transfer values on fluorescence intensity. If the unquenched fluorescence intensity of the donor is independent of the energy transfer, this is reasonable, since the mean energy transfer value would be the same with or without weighting (a more detailed discussion is given in the next section).

In pbFRET we only have pixel-by-pixel photobleaching time constants. We could give pixel-by-pixel energy transfer, if we were able to bleach the donor in a pixel both in the presence and absence of the acceptor. In practice, we measure the photobleaching rate of the donor in the absence (τ_D) and in the presence (τ_{DA}) of the acceptor on separate samples, and calculate the average energy transfer of the double-labeled sample:

$$\bar{E}_{\text{BLEACH}} = 1 - \frac{\overline{\tau_D}}{\overline{\tau_{DA}}} = 1 - \frac{\sum_{k_b}\sum_{k_t} \frac{k_n + k_f}{k_b} \cdot n(k_b, k_t)}{\sum_{k_b}\sum_{k_t} \frac{k_n + k_f + k_t}{k_b} \cdot n(k_b, k_t)} \tag{25}$$

where k_b is the photobleaching rate constant and $n(k_b, k_t)$ is the fraction of pixels with rate constants k_b and k_t. Photobleaching is regarded as a first-order process in our calculations.

We suppose that the number of pixels measured on the donor labeled and donor-acceptor double-labeled sample is the same. If the variation in k_b is negligible as compared to that in k_t, the right side of expression (25) simplifies to the left side of Eq. (26). (A general consideration without simplification is given in the next section). We affirm that $\bar{E}_{\text{BLEACH}} \geq \bar{E}_{\text{INTENSITY}}$, i. e.:

$$\frac{\sum_{l=1}^{M} k_{t,l}}{\sum_{l=1}^{M} (k_{t,l} + k_n + k_f)} \geq \sum_{l=1}^{M} \frac{k_{t,l}}{k_{t,l} + k_n + k_f} \tag{26}$$

where M is the number of pixels. By bringing it to a common denominator and by reduction, we have

$$M + \frac{\sum_{l=1}^{M} \sum_{j=1, j\neq l}^{M} (k_{t,l} + k_n + k_f)^2 \prod_{i=1, i\neq j, i\neq l}^{M} (k_{t,i} + k_n + k_f)}{\prod_{i=1}^{M} (k_{t,i} + k_n + k_f)} \geq M^2 \tag{27}$$

Reduction of the left side gives

$$M + \sum_{l=1}^{M} \sum_{j=1, j\neq l}^{M} \frac{k_{t,l} + k_n + k_f}{k_{t,j} + k_n + k_f} \geq M^2 \tag{28}$$

The left side contains $M \cdot (M-1)/2$ pairs of reciprocal values. It is known that

$$X + \frac{1}{X} \geq 2 \tag{29}$$

where X is an arbitrary positive real number, or in our case:

$$Z = \frac{k_{t,l} + k_n + k_f}{k_{t,j} + k_n + k_f} + \frac{k_{t,j} + k_n + k_f}{k_{t,l} + k_n + k_f} \geq 2 \tag{30}$$

Then inequality (28) can be transformed to the form below:

$$M + \frac{M \cdot (M-1)}{2} \cdot Z \geq M^2 \tag{31}$$

where $Z \geq 2$. Thus, the average energy transfer value calculated by the pbFRET method is larger than that given by the intensity-based method. The greater the difference between $k_{t,l}$ and $k_{t,j}$, the more pronounced the inequality is. This means that the more extensive the heterogeneity in k_t values, the more pronounced is the overestimation.

Monte Carlo simulation of energy transfer calculation according to pbFRET and the intensity-based method

The general form of Eq. (26), without neglecting the variation in k_b, is overwhelmingly complicated, so we preferred to use a computer simulation to analyze this issue. We generated k_b as a normally distributed random variable, and k_t was generated according to a lognormal distribution, since the difference in the average energy transfer values given by the pbFRET and the intensity-based techniques differs markedly in this case, and we often experience a

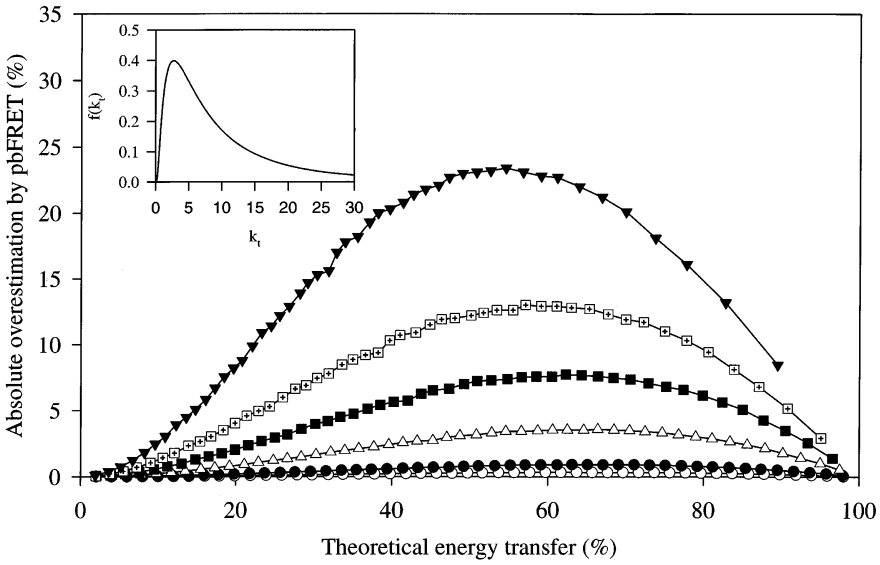

Fig. 5 Comparison of mean energy transfer values calculated according to the intensity-based and the pbFRET technique. The distribution of k_b was supposed to be a normal distribution with a mean of 1000 and a dispersion of 15. The distribution of k_t was a log-normal distribution with σ values of 0.15 (○), 0.25 (●), 0.5 (△), 0.75 (■) and 1 (□). In these cases no weighting on intensities was carried out. In the case of curve marked by +, intensity-based energy transfer values and the bleaching time constants were weighted on the unquenched intensity of the donor. In the case of the curve marked by ▼, intensity-based energy transfer values were weighted according to the quenched intensity, while no weighting was done for the bleaching time constants. The mean value for k_t was varied so that the energy transfer value gave the theoretical energy transfer values on the horizontal axis. The population was sampled 25,000 times by generating random variables with the above distributions. The mean energy transfer values were calculated according to Eqs. (24) and (25). The vertical axis displays the absolute overestimation by the pbFRET technique, that is the difference between the energy transfer value given by the pbFRET and the intensity-based techniques. In the insert the frequency distribution function of k_t when $\sigma = 1$ is displayed

pixel-by-pixel energy transfer distribution similar to the insert in Fig. 5, e. g. in the case of the homoassociation of erbB2 (data not shown). The rate constants of the other de-excitation processes were kept constant. These random distributions were sampled 25,000 times to simulate the measurement of pixel-by-pixel bleaching kinetics of the donor in the presence and absence of the acceptor (Eq. (25)), and to simulate the intensity based measurement of energy transfer (Eq. (24)). We compared the mean energy transfer values that were calculated with the pbFRET and the intensity-based technique (Fig. 5). The overestimation by pbFRET was proportional to the heterogeneity in k_t: the wider the distribution of k_t, the more pronounced the overestimation was. The overestimation was also affected by the energy transfer values: at low energy transfer (below 50%), the overestimation was proportional to the energy transfer.

The effect of weighting the pixel-by-pixel energy transfer values and bleaching time constants on fluorescence intensity was also tested. First we tried to weight either the pixel-by-pixel intensity-based energy transfer values or the bleaching time constants, or both of them, on the unquenched fluorescence intensity of the donor. Neither of the average energy transfer values changed, since we did not incorporate any correlation between the fluorescence intensity and the energy transfer values into our model. Next we tried to weight the intensity-based energy transfer values on the quenched intensity of the donor. We could not carry out a similar weighting with the bleaching time constants, since weighting τ_{DA} on the quenched donor intensity gives τ_D. Since weighting of the intensity-based energy transfer values on the quenched donor intensity introduces a bias towards low energy transfer values (where the donor emission is not quenched), it was not surprising that overestimation by pbFRET was even higher in this case (Fig. 5). We also tried to vary the value of k_b according to a wide distribution, but the overestimation was not significant (data not shown).

Discussion

In the present work we managed to elaborate an intensity-based, quantitative fluorescence microscopic energy transfer method. Our approach is based on accurate background correction and subtraction of spectral overlaps from the energy transfer channel. Comparison between the flow cytometric and the different image cytometric energy transfer calculation methods (Table 3) reveals that we get consistently higher energy transfer values with the pbFRET technique. This overestimation was independent of the pixel size: pixel sizes as large as a cell gave similar results to those obtained with smaller ones, reinforcing the view that energy transfer values are independent of fluorescence intensity in our samples. Some of this discrepancy may be

related to the different weighting of the pbFRET and the intensity-based energy transfer methods (Eqs. (24)–(31)). This overestimation in pbFRET is proportional to the heterogeneity in the pixel-by-pixel energy transfer values. Since the overestimation by pbFRET is higher in the case of the MHCI-MHCII energy transfer pair (FW6/32-RL243) than in the intramolecular energy transfer sample (FL368-R-W6/32), some of the overestimation can be accounted for by Eqs. (24)–(31). We proved that the overestimation by pbFRET is an inherent property of the technique that is related to the different weighting in pbFRET and the intensity-based energy transfer approach. This conclusion was also supported by our Monte Carlo simulation; these studies also showed that the overestimation is proportional to the heterogeneity in the k_t values. Therefore, differences in energy transfer values provided by the pbFRET and the intensity-based approaches should be interpreted with caution.

Although photobleaching is useful in pbFRET measurements, it presents a problem in the case of the intensity-based measurements. So-called antifade agents could have been used to prevent bleaching, but we wanted to compare the intensity-based and the photobleaching energy transfer methods. In addition many of the commercially available antifade agents cause quenching (Molecular Probes) that reduces fluorescence intensity. Furthermore, we must also not forget that any interference with the local environment of membrane proteins may influence their association.

The first step in our calculations is background correction. Having corrected for the constant backgrounds caused by the dark current of the camera and the background fluorescence of the slide and the optical elements of the microscope, we have to take into account the autofluorescence of cells. Since neither fluorescein nor rhodamine has any fluorescence in the ultraviolet range, and cellular autofluorescence is the most intense in this wavelength region, it is convenient to use a UV-excited image for background correction. This approach is identical in theory to the one previously used by us (Szöllősi et al. 1995) to correct images for fluorescence in situ hybridization to detect the faint fluorescence of cosmid probes. In addition, this approach bears some resemblance to the method of Gadella and coworkers (Gadella et al. 1997). They were not lucky enough to have a spectral region where they could acquire a reference image of a labeled sample that contains only cellular autofluorescence. Therefore they had to take images of their labeled sample at two different excitation or emission wavelengths and they also had to determine the ratio of fluorescence intensities of the background and their probe at these wavelengths using an unlabeled sample and a pure solution of their probe, respectively. They could solve their set of equations, that contained linear combinations of probe and background fluorescence, with these ratios.

Important advantages of the intensity-based method are that it requires much less image storing capacity and it is less sensitive to environmental factors than photobleaching (Song et al. 1995, 1996, 1997). The photophysics of bleaching is far from being understood and sometimes pbFRET results give us anomalously high values, especially when we measure energy transfer between very dense cell surface antigens. In the transition region where photobleaching changes from a unimolecular to a bimolecular reaction, the interpretation of results may sometimes be difficult. The sensitivity of pbFRET to environmental factors (such as O_2 concentration) can be alleviated by acceptor photobleaching (Bastiaens et al. 1996; Bastiaens and Jovin 1996), which provides an internal reference for the energy transfer calculations. Since photobleaching of common dyes is irreversible, it is not possible to repeat pbFRET measurements of the same cells. Although the "photobleaching" of some dyes may be reversible, and even controllable (Dickson et al. 1997), such dyes are not widespread and the photophysical processes of this reversibility are not understood. In contrast, intensity-based energy transfer measurements can be repeated several times, and are particularly useful when one wants to follow the kinetics of biological responses.

Accurate determination of energy transfer using the intensity-based microscopic technique requires higher fluorescence intensity than pbFRET does, since sensitized emission is only a small fraction of I_2. The method is also very sensitive to accurate determination of the S factors and the pixel-by-pixel donor/acceptor ratio which also demands high fluorescence intensity. A further drawback of the technique is that the absorption ratio is instrument-dependent, and it may even be altered as the spectral characteristics of the lamp change with time.

A similar method for intensity-based energy transfer calculation has already been published (Kam et al. 1995). Here the authors use the method requiring the determination of an α factor (Trón et al. 1984). However, their method is different from ours in that: *i*) we perform pixel-by-pixel autofluorescence correction; *ii*) we use two, non-competing epitopes on the same protein to ensure that the same amount of antibodies are present for the calculation of α. They drop 2 μL of labeled antibodies onto a slide, dry them and measure the fluorescence intensity. Our method neglects the possibility of minor competition between the two epitopes. Theirs, however, examines the antibodies in a different environment than that they are exposed to during measurements with cells, and it is dependent on accurate measurement of the antibodies and on the drying conditions. Both our method and that of Kam et al. are quantitative, whereas those reported in other publications have used only qualitative or semi-quantitative approaches. In one case, narrow bandpass filters were employed in order to exclude most of the spectral spillage into the energy transfer channel (Uster and Pagano 1986). This method is dependent on these special filters. We mathematically corrected for spectral overlaps, so our method, although a lot more laborious, requires less specific instrumentation. For kinetic measurements they focused on the whole of a single cell and measured the fluorescence intensity using a photomultiplier tube, giving no spatial resolution within the cell. Another approach (Liang et al. 1993) used mathematical algorithms to calculate an energy

transfer image, but pixel-by-pixel correction for the donor-acceptor ratio was not included. This may provide misleading images in cases when the donor and acceptor concentrations show a high degree of heterogeneity (compare Fig. 3 and part *c* of Fig. 4).

Our intensity-based energy transfer calculation method gives reliable and accurate energy transfer values when the fluorescence intensity is reasonably high. It can follow the temporal changes in biological specimens and does not require any special instrumentation, only an image analyzer capable of basic image processing. Such approaches to the association pattern of membrane proteins may shed light on obscure parts of signal transduction that may be related to the spatiotemporal heterogeneity of protein association.

Acknowledgements This work was supported by grants from the Hungarian Academy of Sciences (OTKA F022725, T019372), from the Ministry of Health and Welfare (T-01 344/96) and the Ministry of Education (FKFP 1015/1997).

References

Alberti S, Parks DR, Herzenberg LA (1987) A single laser method for subtraction of cell autofluorescence in flow cytometry. Cytometry 8: 114–119

Bastiaens PI, Majoul JV, Verveer PJ, Soling HD, Jovin TM (1996) Imaging the intracellular trafficking and state of the AB5 quaternary structure of cholera toxin. EMBO J 15: 4246–4253

Bastiaens PI, Jovin TM (1996) Microspectroscopic imaging tracks the intracellular processing of a signal transduction protein: fluorescent-labeled protein kinase C beta I. Proc Natl Acad Sci USA 93: 8407–8412

Beisker W, Dolbeare F, Gray JW (1987) An improved immunocytochemical procedure for high-sensitivity detection of incorporated bromodeoxyuridine. Cytometry 8: 235–239

Damjanovich S, Gáspár R, Pieri C (1997) Dynamic receptor superstructures at the plasma membrane. Q Rev Biophys 30: 67–106

Dickson RM, Cubbit AB, Tsien RY, Moerner WE (1997) On/off blinking and switching behaviour of single molecules of green fluorescent protein. Nature 388: 355–358

Eisinger J (1976) Energy transfer and dynamic structure. Q Rev Biophys 9: 21–33

Gadella TWJ Jr., Vereb G, Hadri AE, Röhrig H, Schmidt J, John M, Schell J, Bisseling T (1997) Microspectroscopic imaging of nodulation factor-binding sites on living Vicia sativa roots using a novel bioactive fluorescent nodulation factor. Biophys J 72: 1986–1996

Hallden G, Skold CM, Eklund A, Forslid J, Hed J (1991) Quenching of intracellular autofluorescence in alveolar macrophages permits analysis of fluorochrome labelled surface antigens by flow cytofluorometry. J Immunol Methods 142: 207–214

Heldin CH (1995) Dimerization of cell surface receptors in signal transduction. Cell 80: 213–223

Jovin TM, Arndt-Jovin DJ (1989) FRET microscopy: Digital imaging of fluorescence resonance energy transfer. Application in cell biology. In: Kohen E, Hirschberg JG (eds) Cell structure and function by microspectrofluorometry. Academic Press. San Diego, CA, pp 99–1117

Kam Z, Volberg T, Geiger B (1995) Mapping of adherens junction components using microscopic resonance energy transfer imaging. J Cell Sci 108: 1051–1062

Liang XH, Volkmann M, Klein R, Herman B, Lockett SJ (1993) Colocalization of the tumor-suppressor protein p53 and human papillomavirus E6 protein in human cervical carcinoma cell lines. Oncogene 8: 2645–2652

Loken MR, Keij JF, Kelley KA (1987) Comparison of helium-neon and dye lasers for the excitation of allophycocyanin. Cytometry 8: 96–100

Seveus L, Vaisala M, Hemmila I, Kojola H, Roomans GM, Soini E (1994) Use of fluorescent europium chelates as labels in microscopy allows glutaraldehyde fixation and permanent mounting and leads to reduced autofluorescence and good long-term stability. Microsc Res Tech 28: 149–154

Shivnan E, Biffen M, Shiroo M, Pratt E, Glennie M, Alexander D (1992) Does co-aggregation of the CD45 and CD3 antigens inhibit T cell antigen receptor complex-mediated activation of phospholipase C and protein kinase C? Eur J Immunol 22: 1055–1062

Song L, Hennink EJ, Young IT, Tanke HJ (1995) Photobleaching kinetics of fluorescein in quantitative fluorescence microscopy. Biophys J 68: 2588–2600

Song L, Varma CA, Verhoeven JW, Tanke HJ (1996) Influence of the triplet excited state on the photobleaching kinetics of fluorescein in microscopy. Biophys J 70: 2959–2968

Song L, van Gijlswijk RPM, Young IT, Tanke HJ (1997) Influence of fluorochrome labeling density on the photobleaching kinetics of fluorescein in microscopy. Cytometry 27: 213–223

Steinkamp JA, Stewart CC (1986) Dual-laser, differential fluorescence correction method for reducing cellular background autofluorescence. Cytometry 7: 566–574

Szabó G Jr, Weaver JL, Pine PS, Rao PE, Aszalos A (1995) Cross-linking of CD4 in a TCR/CD3-juxtaposed inhibitory state: a pFRET study. Biophys J 68: 1170–1176

Szöllősi J, Trón L, Damjanovich S, Helliwell SH, Arndt Jovin D, Jovin TM (1984) Fluorescence energy transfer measurements on cell surfaces: a critical comparison of steady-state fluorimetric and flow cytometric methods. Cytometry 5: 210–216

Szöllősi J, Damjanovich S, Balázs M, Nagy P, Trón L, Fulwyler MJ, Brodsky FM (1989) Physical association between MHC class I and class II molecules detected on the cell surface by flow cytometric energy transfer. J Immunol 143: 208–213

Szöllősi J, Lockett SJ, Balázs M, Waldman FM (1995) Autofluorescence correction for fluorescence in situ hybridization. Cytometry 20: 356–361

Trón L, Szöllősi J, Damjanovich S, Helliwell SH, Arndt Jovin DJ, Jovin TM (1984) Flow cytometric measurement of fluorescence resonance energy transfer on cell surfaces. Quantitative evaluation of the transfer efficiency on a cell-by-cell basis. Biophys J 45: 939–946

Uster PS, Pagano RE (1986) Resonance energy transfer microscopy: observations of membrane-bound fluorescent probes in model membranes and in living cells. J Cell Biol 103: 1221–1234

Young RM, Arnette JK, Roess DA, Barisas BG (1994) Quantitation of fluorescence energy transfer between cell surface proteins via fluorescence donor photobleaching kinetics. Biophys J 67: 881–888

Zhou MJ, Todd RF, 3d, Petty HR (1991) Detection of transmembrane linkages between immunoglobulin or complement receptors and the neutrophil's cortical microfilaments by resonance energy transfer microscopy. J Mol Biol 218: 263–268